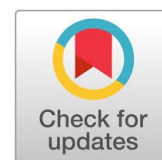




Original Research Article

# Hydrothermal and sol-gel low-temperature synthesis of tin, silver co-doped TiO<sub>2</sub> nanoparticles with enhanced photocatalytic efficiency: artificial neural network modelling



Robab Mohammadi<sup>a,\*</sup>, Mohammad Isazadeh<sup>b</sup>

<sup>a</sup> Department of Chemistry, Payame Noor University, PO BOX 19395-3697, Tehran, Iran

<sup>b</sup> Department of Water Engineering, Faculty of Agriculture, University of Tabriz, Iran

## ARTICLE INFORMATION

Received: 15 August 2018

Received in revised: 1 October 2018

Accepted: 3 October 2018

Available online: 14 January 2019

DOI: [10.33945/SAMI/AJGC.2019.4.2](https://doi.org/10.33945/SAMI/AJGC.2019.4.2)

## KEYWORDS

Ag/Sn-TiO<sub>2</sub> nanoparticles

Sol-gel low-temperature method

Photocatalytic activity

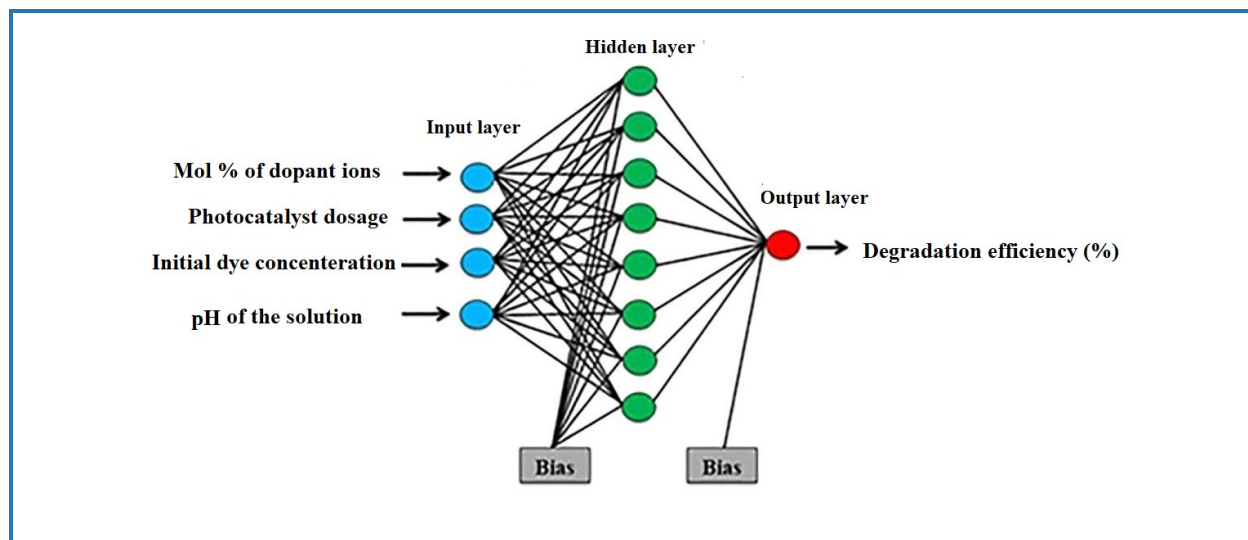
Artificial neural network

## ABSTRACT

Pure anatase TiO<sub>2</sub> nanoparticles with various Ag and Sn contents were synthesized using hydrothermal and sol-gel low-temperature methods. Structural and morphological characterizations of the synthesized nanoparticles were performed by X-ray diffraction (XRD), transmission electron microscopy (TEM), scanning electron microscopy (SEM) equipped with energy dispersive X-ray spectroscopy (EDX), and N<sub>2</sub> adsorption/desorption isotherm and brunauer-emmett-teller (BET) techniques. The effect of synthesis procedure on the crystalline structure, crystal size, surface area, pore size distribution, and photocatalytic activity of the synthesized samples were studied. The photocatalytic activity was tested vs. degradation of methylene blue (MB) under black light radiation. Ag/Sn-TiO<sub>2</sub> nanoparticles synthesized by hydrothermal method showed higher photoactivity during the degradation of MB under black light irradiation due to the increase in the specific surface area, total pore volume, and reducing the crystallite size. An artificial neural network (ANN) comprising four input variables (mol% of dopant ions, photocatalyst dosage, initial dye concentration, and pH of the solution), eight neurons and an output variable (degradation efficiency %) was optimized, tested and validated for MB degradation by Ag/Sn-TiO<sub>2</sub> nanoparticles synthesized *via* hydrothermal method. The results showed that the predicted data from the designed ANN model were found to be in good agreement with the experimental data with a correlation coefficient (R<sup>2</sup>) of 0.979. A 98.9% photodegradation efficiency of MB was achieved by utilizing 0.07 mol% Ag and 0.03 mol% Sn co-doped TiO<sub>2</sub> at pH = 12.

© 2019 by SPC (Sami Publishing Company), Asian Journal of Green Chemistry, Reproduction is permitted for noncommercial purposes.

## Graphical Abstract



## Introduction

During the last decade, application of photocatalysts to control environmental pollution has attracted significant attention from the scientific community as a new environmental purification technique. Among different investigated materials, titanium dioxide ( $\text{TiO}_2$ ) has drawn a lot of interests due to its noticeable chemical stability, low cost, low hazard to human body, strong oxidizing power, and high photoactivity [1–4]. However,  $\text{TiO}_2$  has its own disadvantage including the relatively high speed in recombination of photogenerated electron–hole pairs [5].

To reduce the electron–hole recombination, many studies have been conducted, such as transition metals doping and coupling semiconductors [6]. An effective method for increasing the photocatalytic activity of titanium dioxide is to explore the cooperative influence *via* doping more than one ion metal into  $\text{TiO}_2$  network [7]. Many studies have been conducted towards improving the photocatalytic activity of  $\text{TiO}_2$  [8]. Many studies have been conducted on how to enhance the photocatalytic activity of  $\text{TiO}_2$ . Jeong *et al.* [9] reported the preparation of Cr and Fe co-doped  $\text{TiO}_2$  nanoparticle by hydrothermal synthesis method and showed that Cr and Fe co-doped  $\text{TiO}_2$  nanoparticle have two times higher photocatalytic activity for photodecomposition of gaseous isopropyl alcohol (IPA) than Cr/ $\text{TiO}_2$  and Fe/ $\text{TiO}_2$  nanoparticles under the visible light irradiation ( $\lambda > 420$  nm). Li *et al.* [10] studied the structural and electronic properties of (Fe–F) and (Fe–S) co-doped  $\text{TiO}_2$ . They conclude that the photocatalytic activity of Fe/S  $\text{TiO}_2$  is greater than that of the Fe/F  $\text{TiO}_2$ .

In recent years, artificial neural networks (ANNs) have been employed to simulate the process and define the significance of the different operating variables. Artificial neural networks are

computer based systems designed to simulate the learning process of neurons in the human brain, that has been used in many areas of science and engineering to model different complex processes including biological and physicochemical water/wastewater treatments [11].

Although many researchs have been conducted on various preparation methods for TiO<sub>2</sub> nanoparticles; a comparative research on evaluating the effect of the hydrothermal and sol-gel low-temperature methods on the structure and photocatalytic activity of the samples has not been yet reported. The purpose of this work was to synthesize anatase Ag/Sn-TiO<sub>2</sub> via hydrothermal and sol-gel low-temperature methods and compare the properties of the prepared samples with each other and investigate the relationship between the photocatalyst structure, crystal size, specific surface area, and photocatalytic activity. The influence of different factors such as mol% of dopant ions, photocatalyst dosage, initial dye concentration, and pH of the solution were investigated. Furthermore, the relative importance of each operational parameter was calculated based on the connection weights of ANN model.

## Experimental

### *Materials and Methods*

The following analytical grade chemicals were used without any further purification: titanium n-butoxide (TBOT, Ti (OC<sub>4</sub>H<sub>9</sub>)<sub>4</sub>), glacial acetic acid (AcOH), ethanol with absolute grade, silver nitrate and tin chloride. MB was used as a model compound in the photocatalytic activity measurements. All compounds were supplied from Merck (Germany).

### *Preparation of Ag/Sn-TiO<sub>2</sub> nanoparticles*

#### *Preparation of Ag/Sn-TiO<sub>2</sub> nanoparticles by sol-gel low-temperature method*

In order to synthesize TiO<sub>2</sub> nanoparticles by sol-gel low-temperature method, TBOT was slowly dissolved in AcOH. After stirring for 5 min at 0 °C, distilled water was added drop by drop to the solution under magnetic stirring. The molar ratio of TBOT/AcOH/H<sub>2</sub>O was 1:1:200. The homogeneous solution was yielded after continuously stirred for 1 h. Then, the obtained sol-solution was kept in darkness for 12 h for nucleation process. The obtained solution was placed in an oven at 70 °C for gelation procedure. The gel was then dried at 100 °C for 24 h. Finally, the dry gel powder was calcined at 400 °C for 3 h. Ag/Sn-TiO<sub>2</sub> nanoparticles were synthesized by the same method, except that the water used for the synthesis contained the required amount of AgNO<sub>3</sub> and SnCl<sub>4</sub>. The components of mixed solution are presented in Table 1 (given as molar ratio of doping Ag and Sn).

#### *Preparation of Ag/Sn-TiO<sub>2</sub> nanoparticles by hydrothermal method*

According to [9], Ag/Sn-TiO<sub>2</sub> nanoparticles (Ag 0.07 mol%, Sn 0.03 mol%) were prepared using hydrothermal method. The process involved synthesis of a sol and its hydrothermal treatment. TiO<sub>2</sub> sol was produced from a controlled sol-gel route using TBOT. One molar solution of TBOT in absolute ethanol (5 mL) was added dropwise to 50 mL of distilled water under vigorous stirring. The pH was adjusted to 1.7 with nitric acid. Then TiO<sub>2</sub> sol was added dropwise to the aqueous solutions of AgNO<sub>3</sub> and SnCl<sub>4</sub> in a water bath with continuous stirring. Then the mixture was stirred for 2 h at 50 °C. The mixture finally gained was subjected to a hydrothermal treatment for 5 days at 180 °C and were further calcined at 400 °C for 5 h in an electric furnace to obtain crystalline powders of Ag/Sn-TiO<sub>2</sub>.

#### *Characterization of Ag/Sn-TiO<sub>2</sub> nanoparticles*

The major phase of the samples was determined from X-ray diffraction patterns obtained using a siemens/D5000 diffractometer with Cu K $\alpha$  radiation (0.15478 nm) in the 2 $\theta$  scan range of 20-60°. Average crystallite size (D in nm) of nanoparticles was obtained by Debye-Scherrer's formula given by equation:

$$D = \frac{k\lambda}{\beta \cos\theta} \quad (1)$$

In this equation, K is taken as 0.89;  $\lambda$  is the X-ray wavelength ( $\lambda=0.15406$  nm),  $\beta$  the full width at half maximum intensity and  $\theta$ , the half diffraction angle [8].

The elemental composition, morphology and structure of samples were determined by field emission scanning electron microscope (FESEM, model Philips XL-30 ESM) equipped with an energy dispersive X- ray (EDX). Transmission electron microscopy (TEM) observation was carried out on Philips CM-10 HT electron microscopy instrument operating at 100 kV. BET and BJH measurements were carried out by Belsorp mini II instrument based on N<sub>2</sub> adsorption-desorption. The concentration of MB in all aqueous solutions was analyzed using UV-vis PerkinElmer 550 SE spectrophotometer at wavelengths of 665 nm.

#### *Photocatalytic activity measurement*

Photocatalytic degradation of MB was performed in a batch quartz photoreactor of 100 mL volume with black light lamp (36 W, manufactured by Philips, Holland) emitted around 365 nm positioned above to the reactor [12]. The produced heat from black light lamp was negligible and temperature of the solution during the photocatalytic experiments was nearly constant. In each run, desired amounts of Ag/Sn-TiO<sub>2</sub> catalyst and MB were fed into the reactor and put in the darkness for 30 min in order to establish an adsorption-desorption equilibrium and then exposed to black light

irradiation. At given irradiation time intervals, the sample with a volume of 5 mL was taken out and then analyzed by UV-vis spectrophotometer.

**Table 1.** Molar ratios of Ag/Sn-TiO<sub>2</sub> nanoparticles and degradation efficiency of MB

Sample no.	Ag/Sn Degradation	Efficiency %
1	0/ 0	30
2	0.03/ 0	44
3	0.05/ 0	51
4	0.07/ 0	63
5	0.09/ 0	54
6	0/ 0.01	38
7	0.07/ 0.01	71
8	0.07/ 0.02	80.03
9	0.07/ 0.03	98.9
10	0.07/ 0.07	89
11	0.07/ 0.09	78

## Results and Discussion

### *Characterization of Ag/Sn-TiO<sub>2</sub> nanoparticles*

#### *X-Ray diffraction (XRD)*

X-Ray diffraction (XRD) is a reliable and widespread identification technique especially for crystalline materials [13]. To study the changes in the crystal structure of Ag/Sn-TiO<sub>2</sub> prepared by different methods, XRD analysis was carried out. From Figure 1, all the peaks in the XRD patterns of the samples can be designated to the anatase phase (Most active phase) without any indication of other crystalline phases such as rutile or brookite. High crystallinity of prepared photocatalysts can be conclude from the intensity of the anatase main peak positioned at  $2\theta = 25.5^\circ$  [14]. The crystallite size obtained using Debye-Scherrer's formula for Ag/Sn-TiO<sub>2</sub> nanoparticles prepared by hydrothermal method and Ag/Sn-TiO<sub>2</sub> nanoparticles prepared by sol-gel low-temperature method are 7.2 nm and 9.3 nm, respectively. Absence of a peak corresponding to silver and tin metals may be due to low metal ion dopants content and appropriate dispersion of metal ions on TiO<sub>2</sub> crystal structure [15].

#### *TEM analysis of Ag/Sn-TiO<sub>2</sub> nanoparticles*

TEM image of Ag/Sn-TiO<sub>2</sub> nanoparticles prepared by hydrothermal method is illustrated in [Figure 2a](#). Clear global structure can be observed in TEM image. [Figure 2b](#) shows TEM image of Ag/Sn-TiO<sub>2</sub> nanoparticles prepared by sol-gel low-temperature method. Agglomeration of hydrothermal derived nanopowders is lower than that of sol-gel low-temperature derived nanopowders. As can be seen from TEM image, the average particle size is 8-11 nm. TEM results were in good agreement with that calculated from the XRD pattern using Scherrer equation.

#### *SEM analysis of Ag/Sn-TiO<sub>2</sub> nanoparticles*

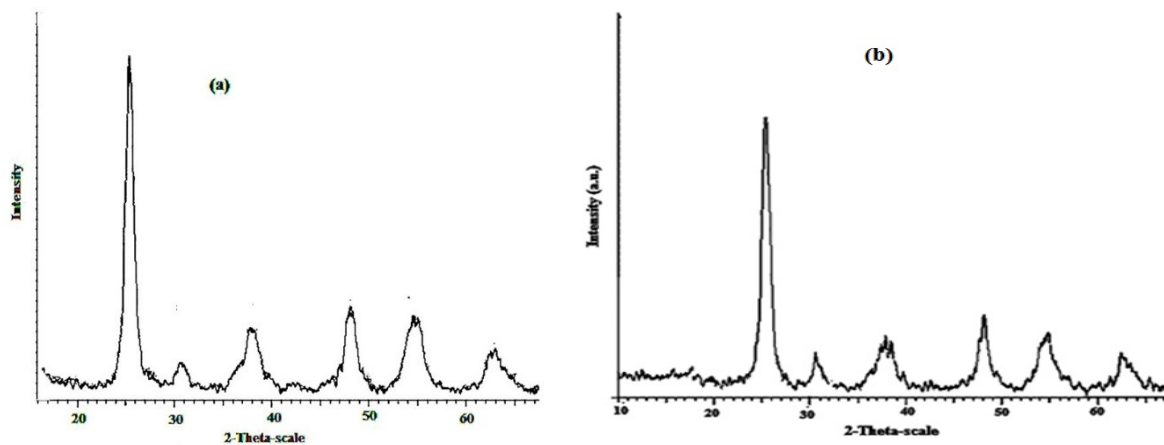
[Figure 3a](#) depicts the SEM image of Ag/Sn-TiO<sub>2</sub> nanoparticles prepared by hydrothermal method. As seen in [Figure 3](#), the nanoparticles are uniformly distributed throughout the sample with rough surface. Spherical morphology with slight agglomeration can be observed for this sample. The SEM image of Ag/Sn-TiO<sub>2</sub> nanoparticles prepared by sol-gel low-temperature method is shown in [Figure 3b](#). This image shows a dense structure particles coherent together. Agglomeration of Ag/Sn-TiO<sub>2</sub> nanoparticles prepared by sol-gel low-temperature is higher than that of Ag/Sn-TiO<sub>2</sub> nanoparticles prepared by hydrothermal method. Since less particle agglomeration occurred for this sample, the large surface area conveys high adsorption abilities of this catalyst [16].

#### *Elemental analysis with EDX spectroscopy*

[Figure 4](#) shows EDX data of Ag/Sn-TiO<sub>2</sub> nanopowders (Ag 0.07 mol%, Sn 0.03 mol%) synthesized via hydrothermal method. TiO<sub>2</sub> shows a peak around 0.5 keV, and another intense peak appears at 4.5 keV. The intense peak is assigned to TiO<sub>2</sub> in the bulk form, and the less intense peak is assigned to TiO<sub>2</sub> surface [19]. The EDX analysis showed Ag and Sn peaks and confirmed the existence of Ag<sup>+</sup> and Sn<sup>2+</sup> of dopants in very low extent. D6t with EDX analysis is due to the uniform and appropriate dispersion of dopants [17].

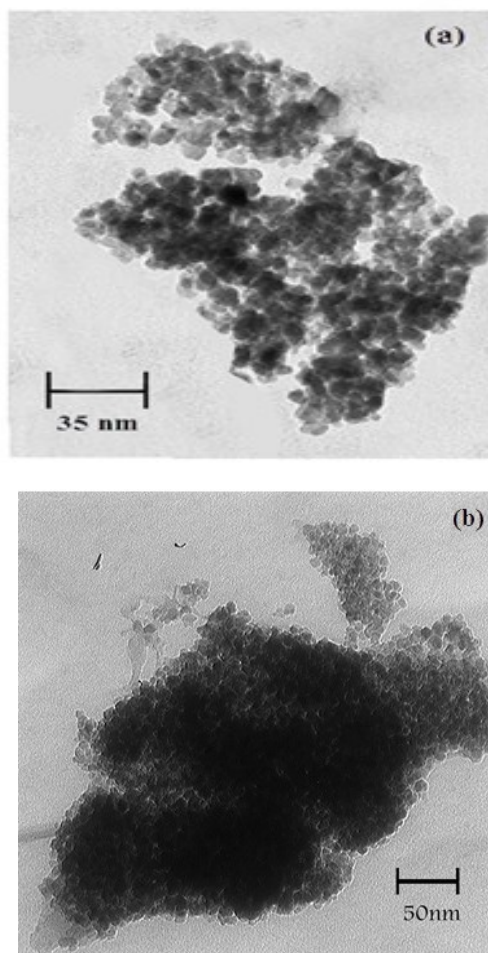
#### *BET analysis*

In order to study the effect of preparation method on specific surface area and porosity of the prepared nanoparticles, N<sub>2</sub> adsorption analysis was carried out. [Figure 5](#) displays the N<sub>2</sub> adsorption-desorption isotherms of Ag/Sn-TiO<sub>2</sub> nanoparticles (Ag 0.07 mol%, Sn 0.03 mol%) prepared by hydrothermal and sol-gel low-temperature methods. Both samples show Type IV isotherm according to IUPAC classifications suggesting the presence of mesoporous structure.



**Figure 1.** XRD patterns of Ag/Sn-TiO<sub>2</sub> nanopowders synthesized *via* a) hydrothermal and b) sol-gel low-temperature methods

**Figure 2.** TEM images of Ag/Sn-TiO<sub>2</sub> nanopowders synthesized *via* a) hydrothermal and b) sol-gel low-temperature methods.



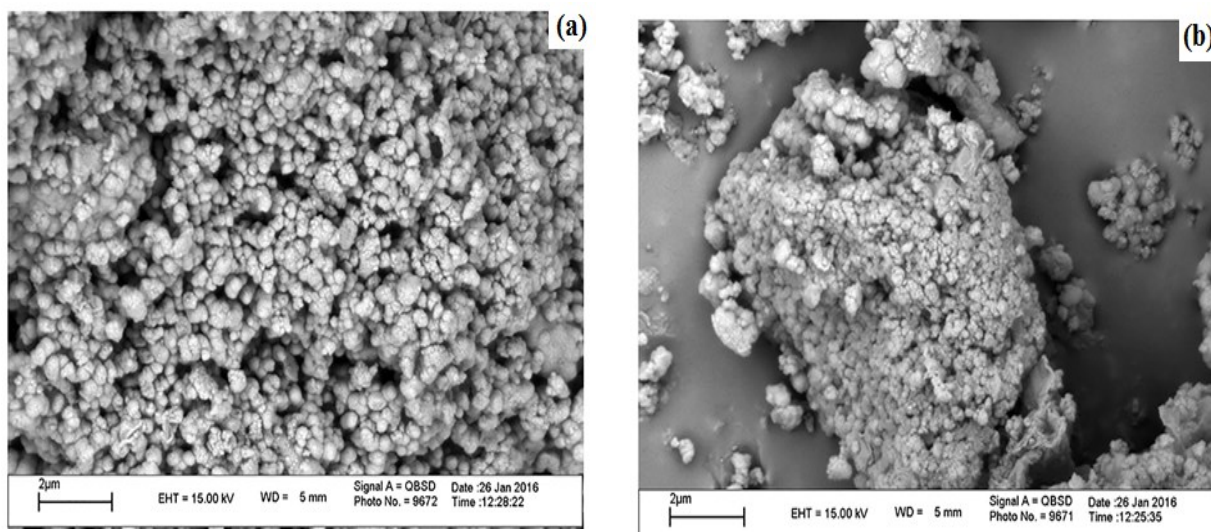


**Figure 3.** SEM images of Ag/Sn-TiO<sub>2</sub> nanopowders synthesized *via* a) hydrothermal and b) sol-gel low-temperature methods

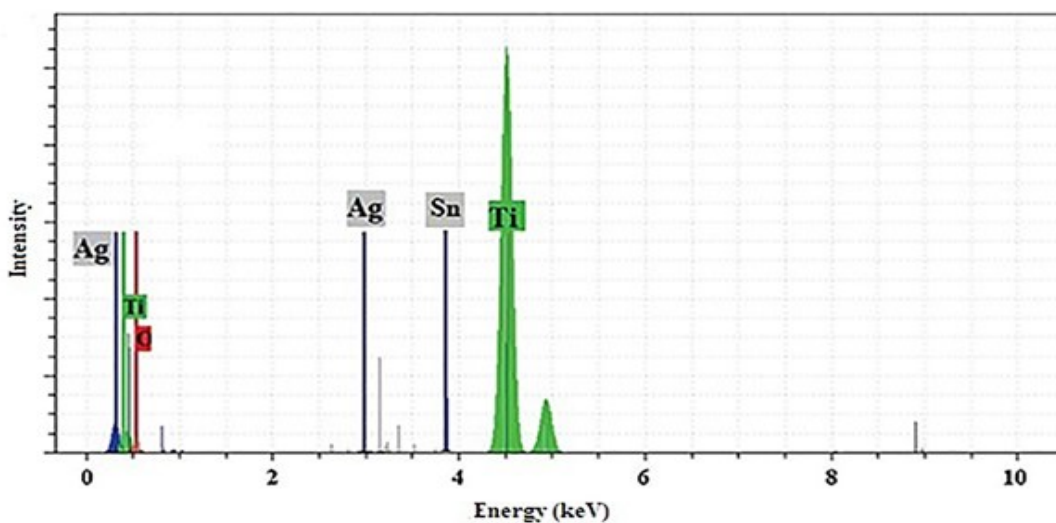


**Figure 4.** EDX spectra of Ag/Sn-TiO<sub>2</sub> nanopowders synthesized *via* hydrothermal method

At high relative pressures from 0.4 to 1, the isotherms showed a Type H<sub>2</sub> hysteresis loop associated with narrow necks and wider bodies (Ink bottle pores), implying that the nanoparticles contain mesopores because of the aggregation of crystallites [18]. The narrow pore size distribution curves indicate that the powders contain uniform pore channels in the mesoporous region [19]. The hysteresis loop in the lower relative pressure range ( $0.5 < P/P_0$ ) was related to finer intra-aggregated pores produced between intra agglomerated primary particles, while the higher relative pressure range ( $0.8 < P/P_0 < 1$ ) was associated with larger interaggregated pores formed *via* interaggregated

secondary particles [20]. Porous structure can facilitate the transporting of reactants and products through the interior space because of the interconnected porous networks, helping the harvesting of exciting light because of the enlarged surface area and multiple scattering within the porous framework [19].

The average pore size distribution estimated according to the BJH method for Ag/Sn-TiO<sub>2</sub> nanoparticles produced *via* hydrothermal and sol-gel low-temperature methods are presented in the Figure 6. The diameter range of the pores was found to be from 1.5 nm to 10 nm with a maximum of 8.4 nm and 10.2 nm for Ag/Sn-TiO<sub>2</sub> nanoparticles prepared by hydrothermal and sol-gel low-temperature methods, respectively. The mean pore diameter of Ag/Sn-TiO<sub>2</sub> nanoparticles prepared by hydrothermal method was less than of the one produced by sol-gel low-temperature method. This was due to the fact that, the smaller pores can be produced *via* the aggregation of smaller crystallites.

BET surface area and total pore volume for Ag/Sn-TiO<sub>2</sub> nanoparticles prepared by hydrothermal method were 136.9 m<sup>2</sup>.g<sup>-1</sup> and 0.179 cm<sup>3</sup>.g<sup>-1</sup>, respectively, which is higher than 61.5 m<sup>2</sup>.g<sup>-1</sup> and 0.127 cm<sup>3</sup> g<sup>-1</sup> of sol-gel low-temperature derived sample. The enhanced surface area of hydrothermal derived sample compared to sol-gel low-temperature derived nanoparticlisis because of its increase in the mesopore size and mesopore volume [21]. It is known in heterogeneous photocatalysis procedure, higher surface area and pore volume can be helpful in the formation of photogenerated electron and hole pairs. So, heterogeneous photocatalysis can be affected by the surface area and pore structure [22].

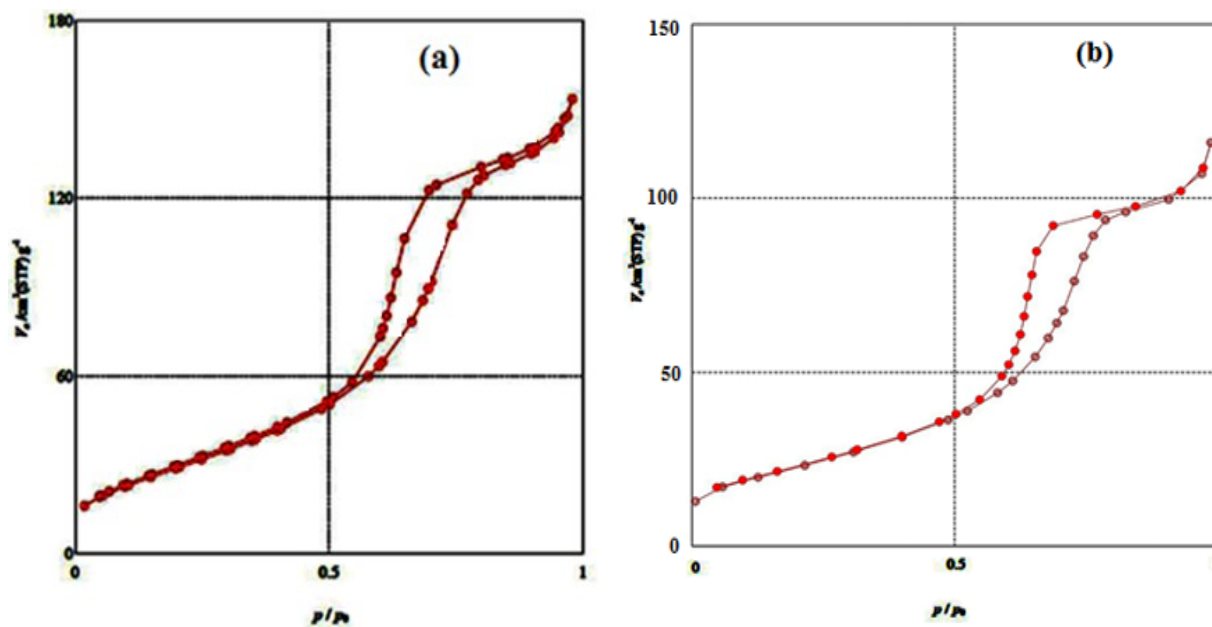


**Figure 5.** Adsorption-desorption isotherms of Ag/Sn-TiO<sub>2</sub> nanopowders synthesized *via* a) hydrothermal and b) sol-gel low-temperature methods

### Photocatalytic activity of prepared samples

Photocatalytic degradation of MB under black light irradiation in the presence of prepared photocatalysts has been listed in Table 1. Results in Table 1 show that photocatalytic activity of Ag/TiO<sub>2</sub> nanoparticles is higher than that of undoped TiO<sub>2</sub>. Direct calcination of the nanoparticles containing silver ions permits formation of silver particles above 400 °C with thermal decomposition process [23]. Thermal decomposition of Ag<sub>2</sub>O to Ag in titanium dioxide system has been reported by Seery *et al.* [24]. Ag loaded on TiO<sub>2</sub> can indirectly change the interfacial charge transfer procedures (ICTP) and also act as an affective electron scavenger [25]. It is known that reduction of electron-hole pair recombination is useful for higher photoactivity. The conduction band of TiO<sub>2</sub> is higher than the Fermi level of Ag which favors the electron transfer from photoexcited TiO<sub>2</sub> to Ag. So, the formation of Schottky barrier is possible in the metallic Ag and TiO<sub>2</sub> contact region [26]. In air-equilibrated systems, Ag discharges the captured electrons into the solution. Therefore, the superoxide and hydroxyl radicals can be formed *via* the reaction of these electrons with dissolved oxygen [27]. However, a reduction in the photocatalytic activity can be observed when the content of silver becomes too large. The detrimental influence of Ag on titanium dioxide photoactivity can be discussed by following reasons:

- A surplus amount of silver dopant can form the recombination center of e<sup>-</sup>-h<sup>+</sup> photoinduced pairs. Recombination of electron and hole pairs decreases the rate of photocatalytic degradation [28, 29].
- Excessive coverage of titanium dioxide restricts the amount of light reaching to the titanium dioxide surface, decreasing the number of photogenerated electron and hole pairs and so, reducing titanium dioxide photoactivity [30].
- Occupation of active sites on the TiO<sub>2</sub> surface by doped silver leads to reduce in the photoactivity of TiO<sub>2</sub> [31].
- The possibility of the hole capture is enhanced by the large number of silver particles at high silver doping reduces the possibility of holes reacting with adsorbed species at the titanium dioxide surface [32].

Furthermore, the influence of tin dopant concentration on photocatalytic activity of Ag-Sn-TiO<sub>2</sub> in the fixed Ag content at optimum value (0.07 mol%) is shown in Table 1. Doping of small amount of tin (up to 0.03 mol%) increased the photocatalytic activity. The oxidation ability of the photoinduced holes of SnO<sub>2</sub> was higher than that of TiO<sub>2</sub> since the valance band position of SnO<sub>2</sub> is lower than that of TiO<sub>2</sub> [23]. Also, the CB of SnO<sub>2</sub> (+0.07 V vs. NHE) has been reported to be located considerably more positive side than that of TiO<sub>2</sub> (-0.34 V vs. NHE), photoinduced electrons easily transfer from TiO<sub>2</sub> to SnO<sub>2</sub> and so, the separation rate of photoinduced electron-hole pairs can be decreased [24]. However, at high tin doping, the excessive Sn species act as a significant center for electron-hole recombination

[21]. From this Table, the highest degrading rate of MB can be observed for Ag-Sn-TiO<sub>2</sub> photocatalyst containing 0.07 mol% Ag and 0.03 mol% Sn.

Lower optimum value for tin in the co-doped system is related to the presence of Ag in the adjacent of Sn. Ionic radius of doped metal ion can significantly affect photoactivity of TiO<sub>2</sub> [31]. Doped metal ions with higher ionic radius than Ti<sup>4+</sup> (Such as silver) in the interstitial positions are more helpful in photoactivity than the metal ions with ionic radius close to Ti<sup>4+</sup> (Such as tin) which can occupy the substitutional positions. Better charge separation and lower electron-hole recombination can be caused by doped metal ions in the interstitial positions. According to these studies, silver in the interstitial positions and zinc in the substitutional positions can separately capture photoinduced electrons and prevent e<sup>-</sup>-h<sup>+</sup> pairs recombination and consequently improve photocatalytic activity.

#### *Influence of synthesis procedure on the photoactivity of Ag-Sn-TiO<sub>2</sub> nanopowders*

It is accepted that the photocatalytic activity of the photocatalyst depends on the morphology, crystallization, total pore volume, and surface area of the material [2, 9, 23, 26, 27]. Ag-Sn-TiO<sub>2</sub> nanopowders prepared by hydrothermal method have better crystallization, which promoted the photocatalytic activity of samples. It is well known that electron-hole recombination rate depends on the particle size [31, 32]. Particle size as a main parameter can influence photocatalytic activity. Small modifications in particle sizes lead to greater variations in the surface/bulk ratio, thus affecting the recombination rates of volume and surface electrons and holes [33]. Hydrothermal-derived nanopowders with small particle size can decline e<sup>-</sup>-h<sup>+</sup> recombination rate. Also, higher photocatalytic activity of hydrothermal-derived nanopowders could be attributed to larger surface area and total pore volume compared to sol-gel derived nanopowders. Large specific surface area leads to adsorb more dyes onto the surface of photocatalyst, while high pore volume (Mesopores) leads to diffuse faster of various liquid reactants and products during the photocatalytic process [34, 35]. According to these results, the hydrothermal preparation method can produce photocatalyst with better efficiency.

#### *Artificial neural network modeling*

Artificial neural networks (ANN) are relatively crude electronic models based on the neural structure of human brain. Artificial neural networks consist of simple processing units called neurons. In this study, a three-layered back propagation ANN was selected, comprising an input layer (Independent variables), an output layer (Dependent variable), and a hidden layer. The number of input and output neurons is determined by the nature of the problem. The hidden layers act like feature detectors; there can be more than one hidden layer. The topology of an artificial neural

network can be achieved through the number of layers in the artificial neural network, the number of nodes in each layer and the nature of the transfer functions. In designing ANN model for a process, suitable identification of the set of independent input variables and the output variables is the first step. The second task in the development of the model is optimization of ANN topology [37]. A three-layered back-propagation algorithm with tangent sigmoid transfer function (Tansig) was employed to activate hidden layer, while a linear transfer function (Purelin) for the input/output layers. All ANN calculations were carried out using Matlab mathematical software, 2011 a version with ANN toolbox.

### *Modeling of operational variables*

The input variables used in the present study were mol% of dopant ions, catalyst amount, initial dye concentration, and pH of the solution. The corresponding degradation efficiency (%) was used as an output of the network. Table 2 presents the ranges of operational parameters.

Artificial neural network used experimental data sets in various conditions to test training. The experimental data sets were split into training (1/2), validation (1/4) and test (1/4) subsets. All inputs and target data must be scaled within a specified range. Therefore, all data ( $X_i$ ) were scaled ( $x_i$ ) into the 0.2–0.8 ranges, through equation 3 [38].

$$x_i = 0.2 + \frac{0.6(X_i - X_{min})}{(X_{max} - X_{min})} \quad (2)$$

Where  $X_{min}$  and  $X_{max}$  refer to the lowest and the highest value of the input variable  $X_i$ , respectively.

The performance of ANN model is affected by the number of neurons in the hidden layer. To determine the optimum number of neurons needed to construct the ANN, a series of topologies were employed in which the number of neurons was varied between 1 and 11. Each topology was repeated 3 times to avoid random correlation due to the random initialization of the weights. Optimization was based on minimizing the mean square error, MSE, which is defined as follows:

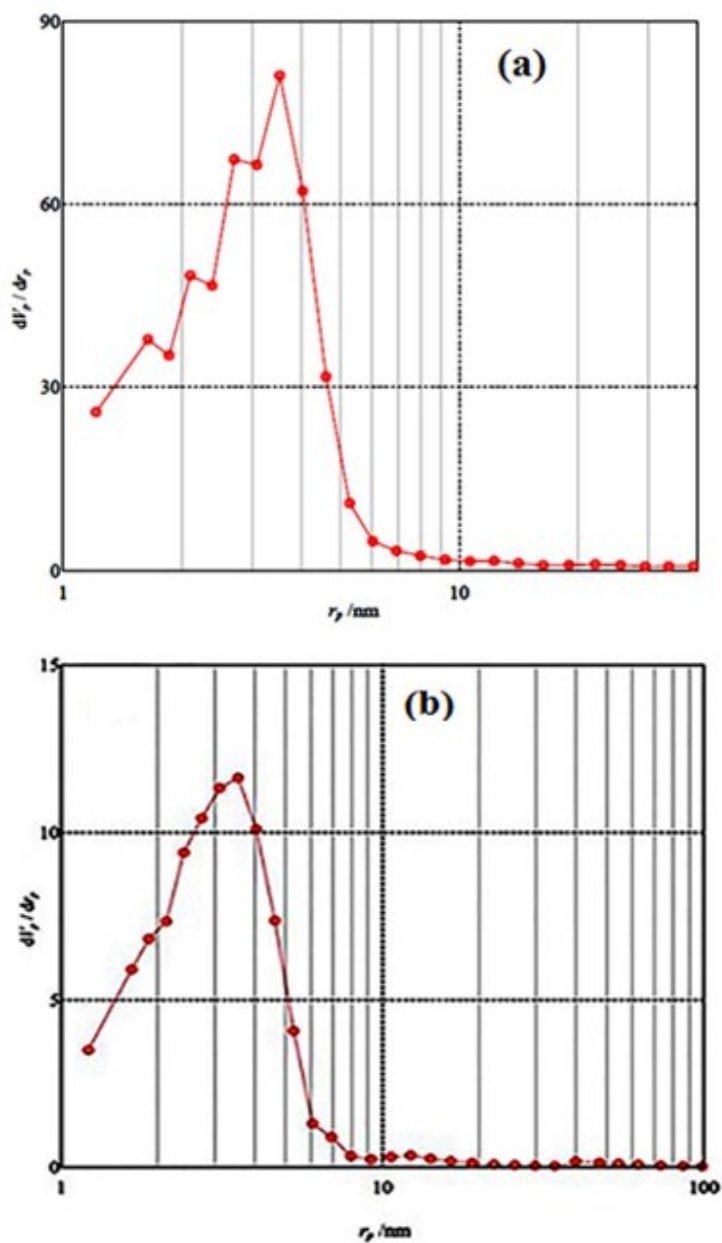
$$MSE = \frac{\sum_{i=1}^{i=N} (t_i - a_i)^2}{N} \quad (3)$$

Where  $t_i$  and  $a_i$  are the predicted and experimental values of the dependent variable, respectively and  $N$  is the number of data. The relationship between the mean square error (MSE) and the number of neurons in the hidden layer is shown in Figure 7. AS can be observed that the performance of the network stabilized after inclusion of an adequate number of hidden units just about eight; therefore,

**Table 2.** The ranges of input and output variables

Variable	Range of the parameter value
Input layer mol% of dopant ions	0-0.09
Photocatalyst dosage ( $\text{g L}^{-1}$ )	0.1-0.6
Initial dye concentration ( $\text{mg L}^{-1}$ )	10-70
pH of the solution Output layer	2-12
Degradation efficiency (%)	12-100

**Figure 6.** Pore diameter distribution of Ag/Sn-TiO<sub>2</sub> nanopowders synthesized via a) hydrothermal and b) sol-gel low-temperature methods



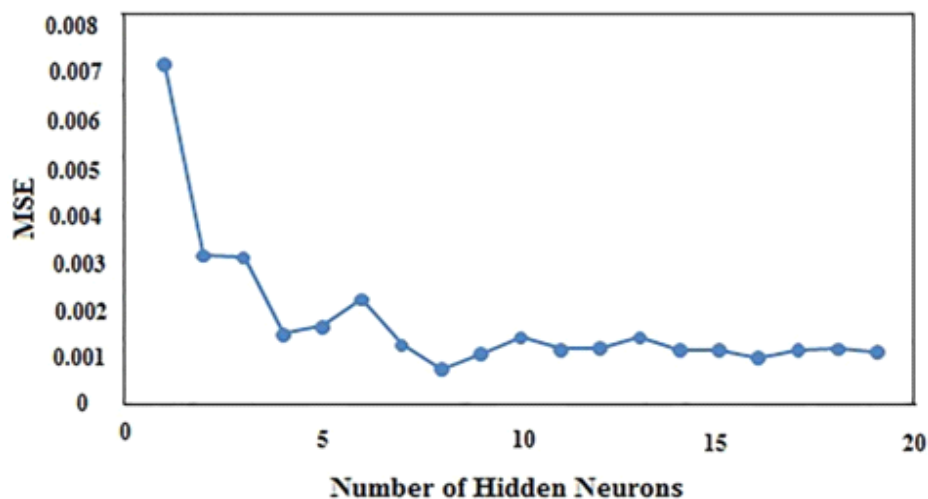


**Figure 7.** Effect of the number of neurons in the hidden layer on the performance of the neural network

8 neurons were selected for the best performance of neural network model. The resulting ANN is schematically illustrated in [Figure 8](#).

[Figure 9](#) shows a comparison between experimental and predicted removal efficiency (%) values for the test set by using ANN model. The plots in these Figures have correlation coefficient ( $R^2$ ) of 0.979 for MB dye. From this plots, it can be conclude that the results obtained from the models are in good agreement with the experimental data, and the model accurately predicts removal efficiency of MB under various conditions.

#### *Optimization and modeling of operational parameters*

To optimize the operational parameters in the photocatalytic degradation of MB by using Ag/Sn-TiO<sub>2</sub> nanoparticles (Sample 9), four operational parameters, mol% of dopant ions, photocatalyst dosage, initial dye concentration, and pH of solution were investigated.

#### *Effect of dopant ions on photocatalytic activity*

In order to investigate the effect of dopant ions on the photocatalytic activity of Ag/Sn-TiO<sub>2</sub> nanoparticles, several tests for degradation of MB was performed under black light irradiation in the presence of 0.4 g.L<sup>-1</sup> of prepared catalysts. The experimental results are presented in [Figure 10](#). It can be seen that doping of TiO<sub>2</sub> with Ag and Sn significantly enhances the photocatalytic efficiency as compared to undoped TiO<sub>2</sub>. Ag/Sn-TiO<sub>2</sub> nanoparticles require less irradiation time than TiO<sub>2</sub> nanoparticles, which can be discussed by following factors. First, it is considered that particle size is a main parameter influencing photocatalytic efficiency, since the electron-hole recombination rate

may depend on the particle size. Partial variations in particle size lead to significant modifications in the surface/bulk ratio, thus influencing the recombination rate of volume and surface electrons and holes [39, 40]. Ag/Sn-TiO<sub>2</sub> with small particle size can decrease the electron-hole recombination rate. Second, this may be due to the fact that a small amount of Ag and Sn ions can trap photo-generated electrons and inhibit the hole-electron recombination [41].

The photocatalytic mechanism involves the excitation of valence electrons to the conduction band by black light illumination, resulting in the formation of holes in the valence band. These species can undergo subsequent reduction and oxidation reactions. In fact, the photocatalytic efficiency depends on the competition between the surface charge carriers transfer rate and the electron-hole recombination rate. If the recombination rate is so fast, there is not enough time for any other reactions to occur, namely there is no photocatalytic activity [42]. These ejected electrons can be trapped by the metal ions co-doped into TiO<sub>2</sub> lattice and the recombination process is holding up. The electrons transfer to the adsorbed oxygen molecules *via* the conduction band of TiO<sub>2</sub> and then trapped through formation of superoxide radical anions. The superoxide radicals and the trapped electrons can combine to produce H<sub>2</sub>O<sub>2</sub>, finally forming hydroxyl radicals. Both hydroxyl radicals and superoxide radical anions are strong oxidants which can oxidize the organic molecules (MB) on the surface of photocatalyst, resulting in the formation of intermediate organic species and subsequently complete oxidation of these species to water and carbon dioxide. Moreover, positive holes in the valence band act as good oxidizing agents available for removal of dye in the solution, •OH (or h<sup>+</sup><sub>vb</sub>) where 'dye' is the pollutant, an electron donor. The photocatalytic performance of co-doped sample was higher than that of undoped TiO<sub>2</sub> for degradation of MB under black light irradiation. Obviously, the photocatalytic activity of Ag and Sn co-doped TiO<sub>2</sub> under black light irradiation demonstrated that Ag and Sn co-doping effect was most outstanding, apparently due to the synergistic effects of Sn<sup>2+</sup> and Ag<sup>+</sup> ions that reduce the recombination of photogenerated electrons and holes, herein enhancing the photoreaction activity of TiO<sub>2</sub> nanoparticles. So, the photocatalytic efficiency of TiO<sub>2</sub> nanoparticles can be enhanced with the presence of an electron acceptor, such as oxygen molecules or metal ions (M<sup>n+</sup>), such as Sn<sup>4+</sup> and Ag<sup>+</sup>, because the recombination of electron/hole pairs can be decreased. Figure 11 depicts that the neural network model correctly predicts degradation efficiency % of MB in the presence of Ag/Sn-TiO<sub>2</sub> nanoparticles as a function of mol% of dopants.

#### *Effect of the amount of Ag/Sn-TiO<sub>2</sub> nanoparticles on photoactivity*

The photocatalytic degradation of MB (20 mg L<sup>-1</sup>) with different Ag/Sn-TiO<sub>2</sub> amounts (Sample 9) was investigated. It is clear from Figure 12 degradation rate of MB was enhanced with the increase of Ag/Sn-TiO<sub>2</sub> up to 0.4 g.L<sup>-1</sup> and 98.9% degradation was achieved after 5 min illumination time. This

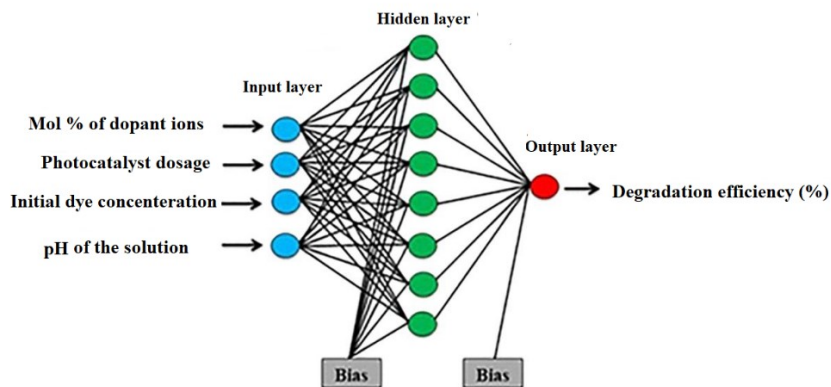


**Figure 8.** Schematic illustration of the optimized ANN structure

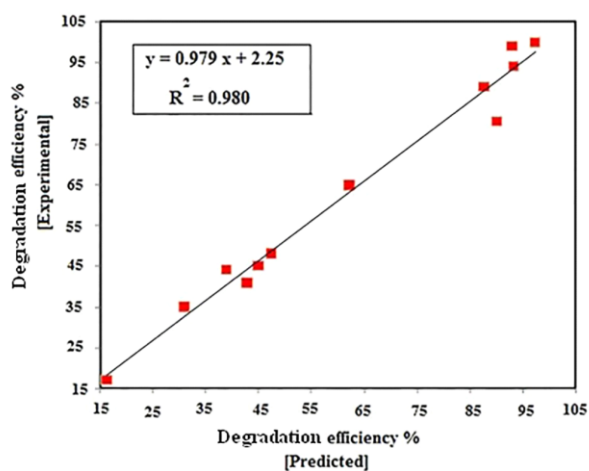


**Figure 9.** Comparison between ANN predicted and experimental degradation efficiency (%) values for the test set of MB degradation

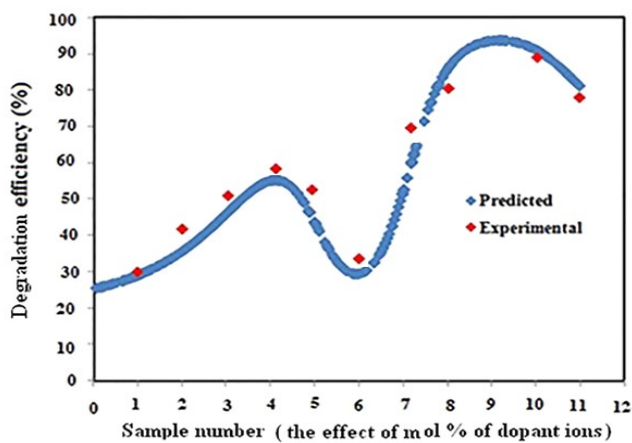


**Figure 10.** Effect of mol% of dopant ions on degradation efficiency of MB (Photocatalyst dosage:  $0.4 \text{ g L}^{-1}$  dye concentration:  $20 \text{ mg L}^{-1}$ , pH: 12).

can be explained in terms of availability of active sites on Ag/Sn-TiO<sub>2</sub> surface and light penetration of photoactivating light into the dye photocatalyst suspension.

At Ag/Sn-TiO<sub>2</sub> amount more than 0.4 g.L<sup>-1</sup>, the percentage of photocatalytic degradation was decreased due to the scattering of light by excess of Ag/Sn-TiO<sub>2</sub> [44]. Another reason is that agglomeration of nanoparticles causes penetration of light becomes hardly to reach all the nanoparticles [47]. So, the degradation efficiency is decreased. In this work, the optimum amount of Ag/Sn-TiO<sub>2</sub> at all subsequent tests conducted was about 0.4 g.L<sup>-1</sup>. Figure 11 shows a good agreement between the degradation efficiency % of MB calculated from the ANN model and the experimental results as a function of photocatalyst dosage.

#### *Effect of the initial MB concentration in the photoreaction*

In order to study the effect of initial dye concentration, experiments were carried out by varying MB concentration from 10 to 70 mg L<sup>-1</sup>, and the degradation efficiency is illustrated in Figure 13. As the initial dye concentration enhances, the degradation efficiency decreases. The possible reason is that direct contact between generated holes or OH• radicals with dye molecules is decreased with increasing the dye concentration due to adsorb of more dye molecules on the surface of Ag/Sn-TiO<sub>2</sub>. By increasing the internal optical density, the solution becomes impermeable to black light [48, 49]. Also, by increasing the dye concentration, MB molecules absorb light and the photons cannot reach Ag/Sn-TiO<sub>2</sub> surface. Therefore the photocatalytic degradation efficiency decreases [50–52]. Figure 12 shows a good agreement between the degradation efficiency % of MB calculated from the ANN model and the experimental results as a function of initial dye concentration.

#### *Effect of pH in the photoreaction*

In this research, the effect of pH in the range from 2 to 12 on degradation efficiency of MB has been investigated because of dependence of both MB molecules and the surface of Ag/Sn-TiO<sub>2</sub> nanoparticles to pH. As seen in Figure 13, an increase in the pH value to 12 caused a significant increase on degradation rate of MB. The influence of pH on the degradation rate of MB in the existence of Ag/Sn-TiO<sub>2</sub> nanoparticles (Sample 9) may be attributed to the basis of the point of zero charge (pH<sub>pzc</sub>) of photocatalyst which has been reported around 6.8 [53]. Ag/Sn-TiO<sub>2</sub> is positively charged in acidic solution (pH<6.8), whereas it is negatively charged under alkaline conditions (pH>7.0). MB is a cationic dye and so, electrostatic interactions between the positive Ag/Sn-TiO<sub>2</sub> surface and MB molecules lead to the strong repulsion of each other. Therefore, under the acidic condition, MB molecules cannot be adsorbed on Ag/Sn-TiO<sub>2</sub> surface [51]. MB degradation is more favorable under alkaline condition because of the formation of more OH and electrostatic attractive effects between

**Figure 11.** Effect of photocatalyst dosage on degradation efficiency of MB (0.07 mol% Ag and 0.03 mol% Sn , dye concentration: 20 mg L<sup>-1</sup>, pH: 12).

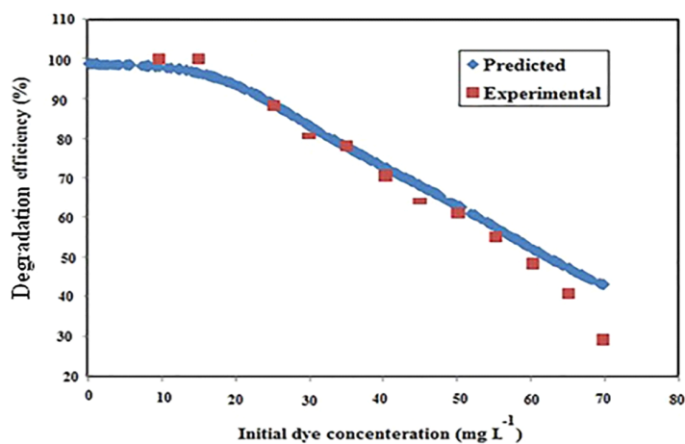
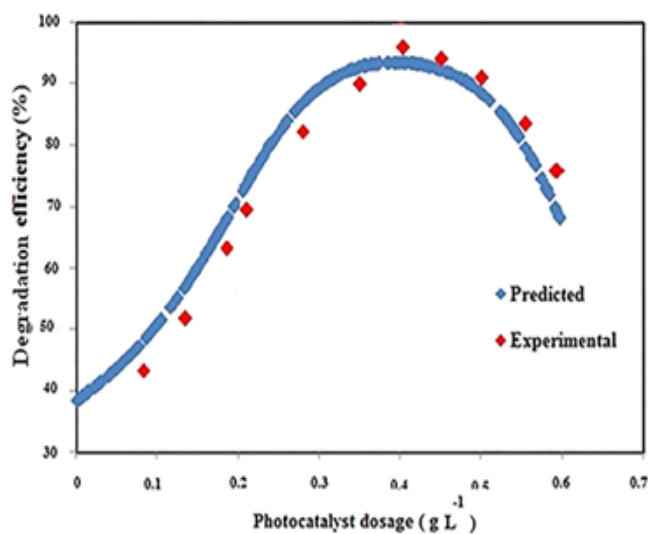


**Figure 12.** Effect of initial dye concentration on degradation efficiency of MB (0.07 mol% Ag and 0.03 mol% Sn , photocatalyst dose: 0.4 g L<sup>-1</sup>, pH: 12)

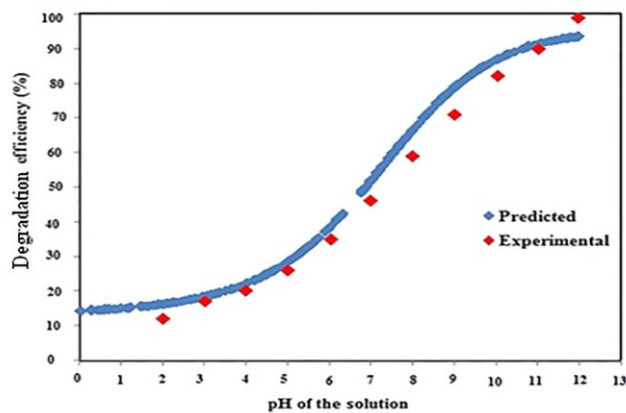


**Figure 13.** Effect of pH value on degradation efficiency of MB (0.07 mol% Ag and 0.03 mol% Sn, photocatalyst dose: 0.4 g L<sup>-1</sup> dye concentration: 20 mg L<sup>-1</sup>)

cationic MB dye and negatively charged surface of Ag/Sn-TiO<sub>2</sub> [52]. Figure 13 shows a good agreement between the degradation efficiency % of MB calculated from the ANN model and the experimental results as a function of pH of the solution.

#### ANN model sensitivity analysis

Table 3 reveals the weights produced by the ANN models used in this work for degradation efficiency of MB. The relative importance of the effect of each input variable on output variable can be obtained through the neural weight matrix [54]. Finally, the relative significance of the input variables was evaluated using the neural weight matrix and the following equation 4 [55]:

$$I_j = \frac{\sum_{m=1}^{m=N_h} \left( \left( \frac{|W_{jm}^{ih}|}{\sum_{k=1}^{N_i} |W_{km}^{ih}|} \right) \times |W_{mn}^{ho}| \right)}{\sum_{k=1}^{k=N_i} \left\{ \sum_{m=1}^{m=N_h} \left( \frac{|W_{km}^{ih}|}{\sum_{k=1}^{N_i} |W_{km}^{ih}|} \right) \times |W_{mn}^{ho}| \right\}} \quad (4)$$

In this equation,  $I_j$  is the relative importance of the  $j^{\text{th}}$  input variable on the output variable,  $N_i$  and  $N_h$  are the number of inputs and hidden neurons, respectively;  $W$ 's are connection weights, the superscripts 'i', 'h' and 'o', respectively, refer to input, hidden and output layers; and subscripts 'k', 'm' and 'n', respectively, refer to input, hidden and output neurons.

Table 4 represents a comparison between the relative importance of input variables as calculated by equation 4 on the degradation efficiency of MB. As shown the importance values of the parameters was pH of the solution > initial dye concentration > mol% of dopant ions > photocatalyst dosage in the selected range of the variables.

**Table 3.** Weight matrix for removal of MB dye: weight between input and hidden layers ( $W_1$ ) and weights between hidden and output layers ( $W_2$ )

Neuron	W1 Input variable mol% of dopant ions				W2 Out put		
	Photocatalyst dosage	Initial dye concentration	pH	bias	Neuron	efficiency %	
1	-0.418	0.156	0.0775	2.281	3.503	1	-0.006
2	0.995	-0.656	0.499	-2.183	-1.571	2	-0.472
3	-2.807	1.748	0.089	-1.645	1.998	3	-2.913
4	1.378	-1.476	0.405	-0.0331	-0.207	4	-1.356
5	1.754	-1.326	2.539	1.612	0.354	5	-2.396

6	1.215	1.060	0.072	1.138	1.599	6	-0.840
7	1.681	0.116	-3.291	0.0366	2.240	7	0.684
8	6.022	0.034	-1.485	0.0319	3.019	8	0.872
						bias	-0.948

**Table 4.** Relative importance of input variables on the value of MB degradation efficiency

Input variable	Importance (%)
mol% of dopant ions	20.3
Photocatalyst dosage (g L <sup>-1</sup> )	18.1
Initial dye concentration (mg L <sup>-1</sup> )	21.5
pH of the solution	40.1

## Conclusion

Ag/Sn-TiO<sub>2</sub> nanoparticles were synthesized by hydrothermal and sol-gel low-temperature methods using titanium *n*-butoxide as precursor. The results implied that photocatalytic activity of Ag/Sn-TiO<sub>2</sub> nanoparticles synthesized *via* hydrothermal method was higher than that of the Ag/Sn-TiO<sub>2</sub> nanoparticles synthesized by sol-gel low-temperature method. TiO<sub>2</sub> co-doped with 0.07 mol% Ag and 0.03 mol% Sn showed highest photocatalytic activity than monometallic doped TiO<sub>2</sub> with Ag, Sn and pure TiO<sub>2</sub> prepared by the same method in the photocatalytic degradation of MB. This might be associated with the effects of co-doped Ag and Sn on the TiO<sub>2</sub> catalyst. The photocatalytic degradation of 20 mg.L<sup>-1</sup> MB was found under 0.4 g.L<sup>-1</sup> of Ag/Sn-TiO<sub>2</sub> and 5 min direct black light illumination. In the present study, the effect of some operational parameters on the photocatalytic degradation of MB was modeled by the ANN technique. A three-layered back-propagation neural network with tangent sigmoid transfer function (Tansig) at the hidden layer with 8 neurons was designed to predict the degradation of MB under various operational conditions. The performance of the synthesized sample in the dye degradation was successfully simulated using neural network modeling, and a good agreement was obtained between the predicted results from the ANN model and the experimental results, with a correlation coefficient (R<sup>2</sup>) of 0.979. The sensitivity analysis showed that the pH of the solution has a larger effect on the photocatalytic degradation of MB, while photocatalyst dosage has the lowest effect on the photocatalytic degradation of MB.

## Acknowledgments

The authors would like to acknowledge the Payame Noor university I. R. of Iran for supporting this project.

## References

- [1]. Kim Y.K., Kim E.Y., Whang C.M., Kim Y.H., Lee W.I. *J. Sol-Gel Sci. Tech.*, 2005, **33**:87
- [2]. Sheikhnejad-Bishe O., Zhao F., Rajabtabar-Darvishi A., Khodadad E., Mostofizadeh A, Huang Y. *Int. J. Electrochem. Sci.*, 2014, **9**:4230
- [3]. Li Y., Jiang Y., Peng S., Jiang F. *J. Hazard. Mater.*, 2010, **182**:90
- [4]. Sun Z., Kim J.H., Zhao Y., Bijarbooneh F., Malgras V., Lee Y., Kang Y.M., Dou S.X. *J. Am. Chem. Soc.*, 2011, **133**:19314
- [5]. Dehghani M., Nasser S., Ahmadi M., Samaei M.R., Anushiravani A. *J. Environ. Health Sci. Eng.*, 2014, **12**:56
- [6]. Nguyen T.B., Hwang M.J., Ryu K.S. *Bull. Korean Chem. Soc.*, 2012, **33**:243
- [7]. Parra R., Ramajo L.A., Go'és M.S., Varela J.A., Castro M.S. *Mater. Res. Bull.*, 2008, **43**:3202
- [8]. Yu C., Cai D., Yang K., Yu J.C., Zhou Y., Fan C. *J. Phys. Chem. Solids.*, 2010, **71**:1337
- [9]. Jeong E.D., Borse P.H., Jang J.S., Lee J.S., Jung O.S., Chang H., Jin J.S., Won M.S., Kim H.G. *Ceramic Process. Res.*, 2008, **9**:250
- [10]. Li X., Lu J., Dai Y., Guo M., Huang B. 2012, *Int. J. Photoenergy*, 2012, **2012**:7 pages
- [11]. Khataee A.R., Kasiri M.B. *J. Molecul. Catal. A: Chem.*, 2010, **331**:86
- [12]. Mohammadi R., Massoumi B. *Russ. J. Phys. Chem. A.*, 2014, **88**:1184
- [13]. Barakat N.A.M., Kanjwal M.A., Chronakis S., Kim H.Y. *J. Mol. Catal. A: Chem.*, 2013, **366**:333
- [14]. Park J.Y., Lee I.H. *J. Nanomater.*, 2014, **2014**:6 pages
- [15]. Mohammadi R., Massoumi B., Rabani M. *Int. J. Photoenergy*, 2012, **2012**:7 pages
- [16]. Mohammadi R. *Desalin. Water. Treat.*, 2016, **57**:22370
- [17]. Ba-Abbad M.M., Kadhum A.A.H., Mohamad A.B., Takriff M.S., Sopian K. *Int. J. Electrochem. Sci.*, 2012, **7**:4871
- [18]. Mohammadi R, Massoumi B., Eskandarloo H., *Desalin. Water. Treat.*, 2015, **53**:1995
- [19]. Bagheri S., Ramimoghdam D., Termeh Yousefi A., Bee Abd Hamid S., *Int. J. Electrochem. Sci.*, 2015, **10**:3088
- [20]. Yao S., Song S., Wang S. *Desalin. Water. Treat.*, 2013, **51**:7101
- [21]. Rivera-Muñoz E.M., Huirache-Acuña R. *Int. J. Mol. Sci.*, 2010, **11**:3069
- [22]. Georgekutty R., Seery M.K., Pillai S.C. *J. Phys. Chem. C.*, 2008, **112**:13563
- [23]. Teoh W.Y., Scott J.A., Amal R. *J. phys. Chem. Lett.*, 2012, **3**:629
- [24]. Seery M.K., George R., Floris P., Pillai S.C. *J. Photochem. Photobiol. A: Chem.*, 2007, **18**:258

- [25]. Liu L., Li Y. *Aerosol. Air Qual. Res.*, 2014, **14**:453
- [26]. Carp O., Huisman C.L., Reller A. *Prog. Solid. State. Chem.*, 2004, **32**:33
- [27]. Zhao B., Chen F., Jiao Y., Yang H., Zhang J. *J. Mol. Catal. A: Chem.*, 2012, **348**:114
- [28]. Sobana N., Muruganadham M., Swaminathan M. *J. Mole. Catal. A.*, 2006, **258**:124
- [29]. Rawal S.B., Ojha D.P., Choi S.Y., Lee W.I. *Bull. Korean Chem. Soc.*, 2014, **35**:913
- [30]. Rawal S.B., Chakraborty A.K., Lee W.I. *Bull. Korean Chem. Soc.*, 2009, **30**:2613
- [31]. Murdoch M., Waterhouse G.I., Nadeem M.A., Metson J.B., Keane M.A., Howe R.F., Llorca J., Idriss H. *Nature. Chem.*, 2011, **3**:489
- [32]. Frontistis Z., Daskalaki V.M., Hapeshi E., Drosou C., Fatta-Kassinos D., Xekoukoulotakis N.P., Mantzavinos D. *J. Photochem. Photobiol. A: Chem.*, 2012, **240**:33
- [33]. Kasiri M.B., Aleboye H., Aleboye A. *Environment. Sci. Technol.*, 2008, **42**:7970
- [34]. Primo A., Corma A., Carsia H. *Phys. Chem. Chem. Phys.*, 2011, **13**:886
- [35]. Sanchooli M., Ghaffari Moghaddam M. *J. Chem. Eng. Japan.*, 2012, **45**:373
- [36]. Emilio C.A., Magallanes J.F., Litter M.I. *Anal. Chim. Acta.*, 2007, **595**:89
- [37]. Abdollahi Y., Zakaria A., Abbasiyannejad M., Fard Masoumi H.R., Ghaffari Moghaddam M., Amin Matori K., Jahangirian H., Keshavarzi A. *Chem. Cent. J.*, 2013, **7**:96
- [38]. Abdollahi Y., Abdullah A.H., Zainal Z., Yusof N.A. *Int. J. Chem.*, 2011, **3**:31
- [39]. Melián E.P., Díaz O.G., Rodríguez J.M.D., Colón G., Navío J.A., Macías M., Pena J.P. *App. Catal. B: Environment.*, 2012, **127**:112
- [40]. Kim H.C., Lee S.H., Kim D.J., Choi J.W. *Wat. Air. Soil. Pollut.*, 2013, **224**:1459
- [41]. Choi J.W., Lee S.Y., Lee S.H., Lee K.B., Kim D.J., Hong S.W. *Wat. Air. Soil. Pollut.*, 2012, **223**:2551
- [42]. [Sin J.C.](#), [Lam S.M.](#), [Mohamed A.R.](#), [Lee K.T.](#) *Int. J. Photoenergy*, 2012, **2012**:23 pages
- [43]. Daneshvar N., Salari D., Khataee A.R. *J. Photochem. Photobiol. A.*, 2003, **157**:111
- [44]. Silva C.G., Juárez R., Marino T., Molinari R., García H. *J. Amer. Chem. Soc.*, 2010, **133**:595
- [45]. Zhao J., Hidaka H., Takamura A., Pelizzetti E., Serpone N. *Langmuir*. 1993, **9**:1646
- [46]. Lodha S., Jain A., Sharma V.K., Punjabi Indonesian P.B. *J. Chem.*, 2008, **42**:42
- [47]. Gomathi Devi L., Kavitha R. *RSC. Adv.*, 2014, **4**:28265
- [48]. Wang H.W., Lin H.C., Kuo C.H., Cheng Y.L., Yeh Y.C. *J. Phys. Chem. Sol.*, 2008, **69**:633
- [49]. Wang W., Zhang J., Chen F., He D., Anpo M. *J. Coll. Interface Sci.*, 2008, **323**:182
- [50]. Liu J., Zhao Y., Shi L., Yuan S., Fang J., Wang Z., Zhang M. *Appl. Mater. Interfaces.*, 2011, **3**:1261
- [51]. Arpac E., Sayilkan F., Asilturk M., Tatar P., Kiraz N., Sayilkan H. *J. Hazard. Mater.*, 2007, **140**:69
- [52]. Subash B., Krishnakumar B., Sreedhar B., Swaminathan M., Shanthi Superlattice M. *Micro.*, 2013, **54**:155
- [53]. Liu J., Xu Z.B. *Adv. Mater. Res.*, 2012, **472**:157

[54]. Garson G.D. *AI. Expert.*, 1991, **6**:47

[55]. Aleboyeh A., Kasiri M.B., Olya M.E., Aleboyeh H. *Dyes Pigm.*, 2008, **77**:288

**How to cite this manuscript:** Robab Mohammadi\*, Mohammad Isazadeh. Hydrothermal and sol-gel low-temperature synthesis of tin, silver co-doped TiO<sub>2</sub> nanoparticles with enhanced photocatalytic efficiency: artificial neural network modelling. *Asian Journal of Green Chemistry*, 3(4) 2019, 432-454. DOI: [10.33945/SAMI/AJGC.2019.4.2](https://doi.org/10.33945/SAMI/AJGC.2019.4.2)